pH-Dependent Perturbation of Ras−Guanine Nucleotide Interactions and Ras Guanine Nucleotide Exchange†

Jongyun Heo,‡ Guanghua Gao,‡ and Sharon L. Campbell*,‡,§

Department of Biochemistry and Biophysics and Lineberger Comprehensive Cancer Center, University of North Carolina, 530 Mary Ellen Jones Building, Chapel Hill, North Carolina 27599-7260

Received September 20, 2003; Revised Manuscript Received May 18, 2004

ABSTRACT: $p21^{Ras}$ (Ras) proteins cycle between active GTP-bound and inactive GDP-bound states to mediate signal transduction pathways that promote cell growth, differentiation, and apoptosis. To better understand how cellular regulatory factors, such as guanine nucleotide exchange factors (GEFs) and nitric oxide (NO), modulate Ras−guanine nucleotide binding interactions, we have conducted NMR and kinetic studies to investigate the pH dependence of Ras−GDP interactions and Ras−guanine nucleotide exchange (GNE). pH-sensitive amide protons were identified and found to be associated with residues in the switch I (Phe^{28}−Asp^{30}) and switch II (Asp^{57} and Thr^{58}) regions of Ras. Furthermore, most of the residues that interact with Mg^{2+} exhibit pH-sensitive amide proton chemical shifts which appear to be coupled to pH-dependent Ras Mg^{2+} binding and guanine nucleotide binding affinity. These results suggest that perturbation of Mg^{2+} interactions within the Ras−guanine nucleotide complex is critical for pH-dependent dissociation of guanine nucleotide ligands from Ras. Notably, these same regions undergo conformational changes upon association with the Ras GEF, SOS. In addition, although we have recently shown that addition of NO to Ras in the presence of oxygen produces a Ras thiyl radical intermediate that promotes Ras GNE, we have also postulated that another byproduct of this reaction, a H^+, may contribute to NO-mediated GNE. However, the results presented herein suggest that the H^+ byproduct of the reaction is unlikely to be involved in the NO-mediated Ras GNE.

The human ras family consists of three proto-oncogenes, H-ras, K-ras, and N-ras, which encode 21 kDa protein products, often termed $p21^{Ras}$ (Ras) (*1*). Ras proteins are localized to the inner plasma membrane, bind guanine nucleotide ligands (GDP and GTP) with high affinity, and possess a slow nucleotide dissociation rate and intrinsic GTPase activity (*1*−*3*). Ras proteins mediate a diverse array of processes, including cellular growth, proliferation, differentiation, and apoptosis (*1*, *3*). Ras exists predominantly in its inactive GDP-bound form in the unstimulated cell (*4*, *5*). A variety of extracellular stimuli such as growth factors and neurotransmitters promote release of GDP and the subsequent binding of GTP. GTP binding, in turn, promotes conformational changes in the Ras switch I and switch II regions that enhance the interaction of Ras with effector molecules. Activation of downstream effectors by Ras−GTP leads to the transmission of intracellular signals, through a plethora of downstream signaling pathways. The signal is subsequently downregulated by hydrolysis of Ras-bound GTP to GDP and inorganic phosphate.

The intrinsic guanine nucleotide exchange and GTP hydrolysis rates of Ras are too slow to modulate Ras activation or deactivation on the time scale of cellular events. To accelerate GTP hydrolysis, needed to downregulate the transient burst of signaling activity mediated by Ras−GTP, regulatory proteins such as GTPase activating proteins (GAPs)[1] bind to the GTP-bound form of Ras and stimulate GTPase activity (*6*). Other types of regulatory proteins, guanine nucleotide exchange factors (GEFs), act to upregulate Ras signaling by stimulating the intrinsically slow guanine nucleotide exchange (GNE) rate (*7*). Nitric oxide (NO) has also been shown to regulate Ras activity by stimulating GNE on Ras (*8*). Nucleotide binding regions of Ras proteins include residues within switch I (broadly defined here as residues 25−40) that interact with nucleotide base, ribose, and γ-phosphate (in the GTP-bound form), the P-loop GxxxxGK(S/T) motif (residues 10−17), the switch II DxxG motif (residues 57−60) that interacts with the phosphate group, and residues 116−119 (NKCD motif) and 145−147 (SAK motif) which interact with the guanine base (*9*, *10*). Comparison of crystal structures of active (Ras−GTP) and inactive (Ras−GDP) forms of Ras revealed conformational changes that were mainly localized to the switch I and switch II regions (*10*). Notably, the switch I region contains the effector-binding region (located between residues 32 and 40)

† This work was supported by NIH Grants RO1CA89614-O1A1 and PO1 HL45100 to S.L.C.

* To whom correspondence should be addressed. E-mail: campbesl@med.unc.edu. Fax: (919) 966-2852. Telephone: (919) 966−7139.

‡ Department of Biochemistry and Biophysics.

§ Lineberger Comprehensive Cancer.

[1] Abbreviations: NH, amide; H_N, amide proton; GAPs, GTPase activating proteins; GEFs, guanine nucleotide exchange factors; GNE, guanine nucleotide exchange; HSQC, heteronuclear single-quantum correlation; NO, nitric oxide; $^{\bullet}NO_2$, nitrogen dioxide; SOS, Son of sevenless. In the Ras superfamily, the residue designated as X in the NKXD guanine nucleotide-binding motif is not conserved. However, in H-, K-, and N-Ras, this residue is cysteine. We, therefore, have used NKCD to describe this guanine nucleotide-binding motif in Ras.

10.1021/bi035704a CCC: $27.50
Published on Web 07/17/2004

and represents an essential element for regulatory interactions with Ras downstream effectors, GEFs and GAP proteins (*3*).

Key binding of proteins and ligands can be divided into two primary types of interactions, electrostatic (including hydrogen bond) and hydrophobic. Analysis of Ras crystal structures shows the presence of multiple intricate hydrogen bond interactions between Mg^{2+}·guanine nucleotide ligand complexes (Mg^{2+}·GTP and Mg^{2+}·GDP) and residues in Ras, indicating that hydrogen bond interactions may constitute the majority of interactions that contribute to high affinity and specific binding of Ras with Mg^{2+}·GDP or Mg^{2+}·GTP (*10*). As such, mechanisms of Ras regulation in which perturbation of hydrogen bond interactions between Ras and its ligand, Mg^{2+}·GDP, leads to decreased Ras nucleotide binding affinity can be envisioned, a mechanism which thereby alters Ras GNE and Ras activity in the cell. Binding of the Ras−GEF (SOS) to the Ras switch I and II regions has been shown to induce conformational changes in Ras, leading to disruption of multiple interactions, including hydrogen bond interactions, between Ras and its Mg^{2+}·nucleotide ligands (*7*). Moreover, like the action of Ras GEFs, treatment of Ras with NO has been shown to facilitate Ras GNE, leading to Ras−GTP loading and activation *in vivo* (*11*). We have recently elucidated the chemical process of Ras NO modification and its relevance to Ras GNE (*12*). On the basis of results from these studies, we have proposed that NO initially reacts with O_2 to produce nitrogen dioxide ($^{\bullet}NO_2$), which in turn reacts with the Ras Cys^{118} thiol (Ras-S^{118}H) to produce a Ras thiyl radical intermediate (Ras-$S^{118\bullet}$) and a proton (H^+). Reaction of Ras-$S^{118\bullet}$ with NO then generates the end product of the reaction, S-nitrosylated Ras (Ras-S^{118}NO). Although the previous study demonstrated that formation of Ras-$S^{118\bullet}$ promotes dissociation of Mg^{2+}·GDP from Ras, it was also postulated that the H^+ byproduct of this reaction may also contribute to Ras−guanine nucleotide dissociation by perturbing pH-sensitive interactions between Ras and its Mg^{2+}·nucleotide ligands, Mg^{2+}·GDP and Mg^{2+}·GTP. Whatever the mechanism of Ras GNE, perturbation of hydrogen bond interactions between Ras and Mg^{2+}·nucleotide ligands is likely an important driving force in facilitating Ras GNE.

We have employed NMR and kinetic approaches to investigate the pH dependence of Ras·Mg^{2+}·GDP interactions and Ras GNE. Our results provide fundamental biophysical information about electrostatic (including hydrogen bond) interactions between Ras and Mg^{2+}·GDP, which in turn provides insight into how perturbation of pH-dependent interactions in Ras promotes GNE. Our studies also provide insight into how modulatory agents such as Ras GEFs and NO regulate Ras nucleotide affinity by perturbing electrostatic Ras·Mg^{2+}·GDP interactions to promote GNE, leading to Ras activation *in vivo*. Our determination of pH-dependent Ras Mg^{2+} affinity provides further mechanistic information about the role of Mg^{2+} in Ras−guanine nucleotide interactions. Altogether, this study provides fundamental yet critical information about binding interactions between Ras and Mg^{2+}·nucleotide ligands, which will aid in understanding GEF-mediated and, further, NO-mediated mechanisms of Ras GNE.

MATERIALS AND METHODS

Preparations of Chemicals, Ras Proteins, and Buffers. The chemicals used for all experiments were of the highest grade unless otherwise noted. 2′(3′)-*O*-(*N*-Methylanthraniloyl)-guanosine 5′-diphosphate (mant-GDP) was purchased from Molecular Probes. A mixed buffer that consists of 10 mM MES, MOPS, Tris-HCl, HEPES, and 50 mM NaCl was used for fluorescence and Mg^{2+} binding studies at various pHs. The mixed buffer was passed through a Bio-Rad Chelex-100 cation exchange resin to remove any trace transition metals, including Mg^{2+} (*13*). Isotope-enriched ([^{13}C,^{15}N]) human Harvey-Ras (H-Ras, residues 1−166) was expressed and purified as described previously (*14*). NMR buffer containing *d*-Tris-maleate (10 mM), $MgCl_2$ (5 mM), NaCl (50 mM), GDP (20 μM), azide (0.001%), and D_2O (10%) was used for NMR−pH titration of Ras.

Acquisition and Analysis of NMR Spectra. All NMR data were acquired using a Varian Inova 600 spectrometer at 298 K. The data were processed and analyzed using NMRpipe and NMRview, respectively (*15*, *16*). Heteronuclear single-quantum correlation (HSQC) NMR spectra, as a function of pH, were acquired by exchanging a ^{13}C- and ^{15}N-enriched Ras sample with NMR buffer that had been adjusted to the desired pH. Briefly, the Ras NMR sample volume was reduced to 100 μL by using a centricon (Millipore). The concentrated NMR sample was then diluted to 2 mL with freshly prepared NMR buffer, at the desired pH. The diluted NMR sample was reconcentrated to 600 μL using a centricon (final concentration of 0.4 mM). Amide (NH) chemical shift assignments were obtained previously (*17*), and were used to assign resonances detected at different pH values by careful inspection of HSQC spectra as a function of pH. The amide proton (H_N) and ^{15}N chemical shift changes at each pH were quantified by using the Pythagorean relation (eq 1) (*18*):

$$\Delta\mathrm{NH} = \sqrt{\Delta H^2 + (\Delta N/6)^2} \qquad (1)$$

where ΔH and ΔN correspond to ^{1}H and ^{15}N chemical shift changes (parts per million) for a particular NH, respectively.

The H_N exchange experiment was initiated by suspending ^{13}C- and ^{15}N-enriched Ras (residues 1−166) in 100% D_2O (pD 6.9), to a final Ras protein concentration of 0.4 mM. The Ras sample was equilibrated at 298 K for 5 min in the NMR spectrometer, and the first HSQC spectrum was acquired 20 min after D_2O exchange was initiated. Because of the time required to prepare the sample and set up the amide exchange experiment, the earliest time point was 20 min. Additional spectra were acquired at 10 min intervals over a time period of 20−970 min. Since the peak intensity of the Gly^{13} NH resonance was insensitive to D_2O exchange over the experimental time period (970 min), volume integrals of all observable NH Ras residues were normalized to the nonexchangeable NH of Gly^{13}. NH exchange rate constants (k_{ex}) were obtained by fitting the decrease in peak intensity as a function of time to a first-order exponential decay using NMRview.

Unlabeled H-Ras (residues 1−166) was used for ^{31}P NMR studies. Buffers and sample preparation protocols for ^{31}P NMR data collection at pH 6.1 and 8.0 were identical to those used for collection of HSQC spectra.

Determination of NH Chemical Shift-Based Apparent pK_as in the Ras·Mg^{2+}·GDP Complex. The chemical shift of the ^{1}H and its attached ^{15}N nucleus can be detected in a two-dimensional ^{1}H−^{15}N HSQC spectrum, and are sensitive to changes in their electrochemical environment and, as such, are sensitive to changes in pH. Given that the pK_a values for protein H_Ns (pK_a > 9) are typically beyond the pH range (5.9−8.0) that was being studied, pH-dependent NH chemical shifts observed for Ras most likely correspond to proximal pH-sensitive titrating groups that alter the electrochemical environment of the NH group that is being investigated. The pK_a values were determined by monitoring pH-dependent NH chemical shifts and reflect pH-dependent changes in the chemical environment of Ras·Mg^{2+}·GDP functional groups proximal to the NH groups that are being investigated. Hence, we will refer to the pK_a values derived from pH-dependent NH chemical shifts as apparent NH pK_a values (^{appNH}pK_a). The ^{appNH}pK_a values for Ras−GDP interacting residues were determined by fitting pH-dependent NH chemical shift changes to the monoprotic Henderson−Hasselbalch equation (*19*). Notably, chemical shift data for pH values of <5.9 and >8.0 were unavailable, since Ras (residues 1−166) is unstable outside the pH range from 5.9 to 8.0. The ^{appNH}pK_a values for certain Ras residues (e.g., Phe^{28} and Val^{29}) were estimated by examining the trend of pH-dependent chemical shifts, since pH-dependent chemical shifts could not be determined over the pH range required for accurate pK_a determination. For instance, significant NH chemical shifts for Phe^{28} were observed between pH 5.9 and 6.5, while minor chemical shifts were observed between pH 6.5 and 8.0. These data indicate that the ^{appNH}pK_a values of Phe^{28} must be less than 5.9 (5.9 > ^{appNH}pK_a).

Determination of the Mg^{2+} Binding Affinity of Ras at Various pHs. The Mg^{2+} binding affinity of Ras was estimated by measuring the dependence of Ras·Mg^{2+}·mant-GDP dissociation rate constants on the Mg^{2+} concentration at various pHs at 25 °C (*20*, *21*). Ras protein samples were dialyzed with metal-free buffer to remove Mg^{2+} ions, and Mg^{2+}-free mixed buffer was used for all Mg^{2+} binding assays.

Analysis of Ras Structures. PDB coordinates for Ras NMR solution structures (1AA9, 1CRQ, and 1CRR for Ras·Mg^{2+}·GDP) and crystal structures (1Q21 and 4Q21 for Ras·Mg^{2+}·GDP and 1QRA for Ras·Mg^{2+}·GTP) were employed for the examination of the Ras·Mg^{2+}·guanine nucleotide ligand structures.

RESULTS

Although the NMR pH titration of H-Ras (residues 1−166) was limited to the pH range from 5.9 to 8.0 due to the instability of Ras·Mg^{2+}·GDP, the pH titration conducted in this study encompasses a physiologically relevant pH regime for Ras. ^{1}H−^{15}N HSQC spectra were acquired on Ras·Mg^{2+}·GDP over a pH range of 5.9−8.0 to determine the amide protons (H_N) in Ras that are sensitive to pH changes. Although pH-dependent amide (NH) chemical shifts are observed for residues outside the guanine nucleotide-binding site (such as Asp^{92} and Gln^{95}), we have focused on pH-dependent NH chemical shifts associated with Ras residues that interact with the Mg^{2+}·nucleotide ligand. As shown in Figure 1, these pH-dependent NH chemical shifts ($\Delta\delta$) are localized to regions of Ras corresponding to the P-loop, switch I and switch II (Figure 1, green circle). These regions of Ras form interactions with Mg^{2+} and the α- and β-phosphates of bound GDP, primarily through hydrogen bonds. In detail, significant pH-dependent NH chemical shift changes corresponding to Ras switch I residues Phe^{28}, Val^{29}, Asp^{30}, and Thr^{35}, as well as switch II residues Asp^{57} and Thr^{58}, were observed over the pH range of 5.9−8.0 (Figure 2 and Table 1). Minor NH chemical shift changes are also observed for P-loop residue Ser^{17} (Figure 2 and Table 1); in contrast, NH chemical shifts associated with residues in the conserved nucleotide base binding motifs (NKCD/SAK) and nucleotide phosphate binding P-loop residues are virtually unchanged (Figures 1 (black circle) and 2 and Table 1).

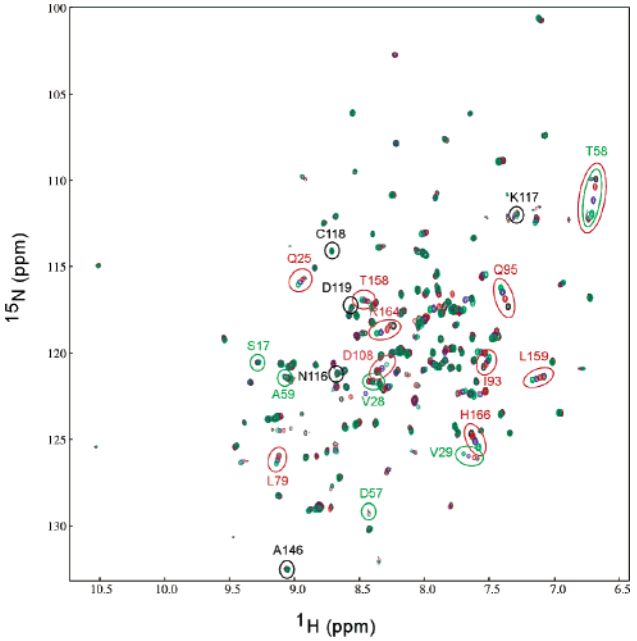

FIGURE 1: HSQC spectra for wild-type Ras (residues 1−166) at various pHs. NMR data procedures for acquisition, spectra processing, and resonance assignments are described in Materials and Methods. Contour plots in black, red, blue, and green correspond to spectra acquired at pH 5.9, 6.5, 7.0, and 8.0, respectively. Most pH-sensitive residues are circled in red. Critical Ras−guanine base interaction residues in Ras NKCD and SAK motifs are denoted with black circles. Ras residues that coordinate Mg^{2+} are circled in green.

Slow H_N exchange rates were observed for residues in the NKCD/SAK motifs, the nucleotide phosphate binding P-loop residues, and switch II residue Asp^{57} (Table 1). In contrast, a moderate H_N exchange rate was observed for switch II residue Thr^{58}, and fast H_N exchange rates were observed for switch I residues (particularly Phe^{28}−Asp^{30}), including Mg^{2+} coordination residues. These NMR results suggest a correlation between residues that possess fast H_N exchange rates and the most pH-sensitive residues in Ras, with the exception of Ser^{17}.

Analysis of pH-Dependent Perturbation of Ras Residues in Switch I. The NMR studies show that the NH resonances corresponding to Ras switch I residues Phe^{28}, Val^{29}, and Asp^{30} are sensitive to changes in pH over the range of 5.9−8.0 (Figure 3 and Table 1), with an estimated ^{appNH}pK_a of <5.9. Analysis of Ras·Mg^{2+}·GDP NMR solution structures (PDB entries 1AA9, 1CRQ, and 1CRR) indicates the presence of multiple electrostatic interactions (including hydrogen bond interactions) associated with the Phe^{28}−Asp^{30}

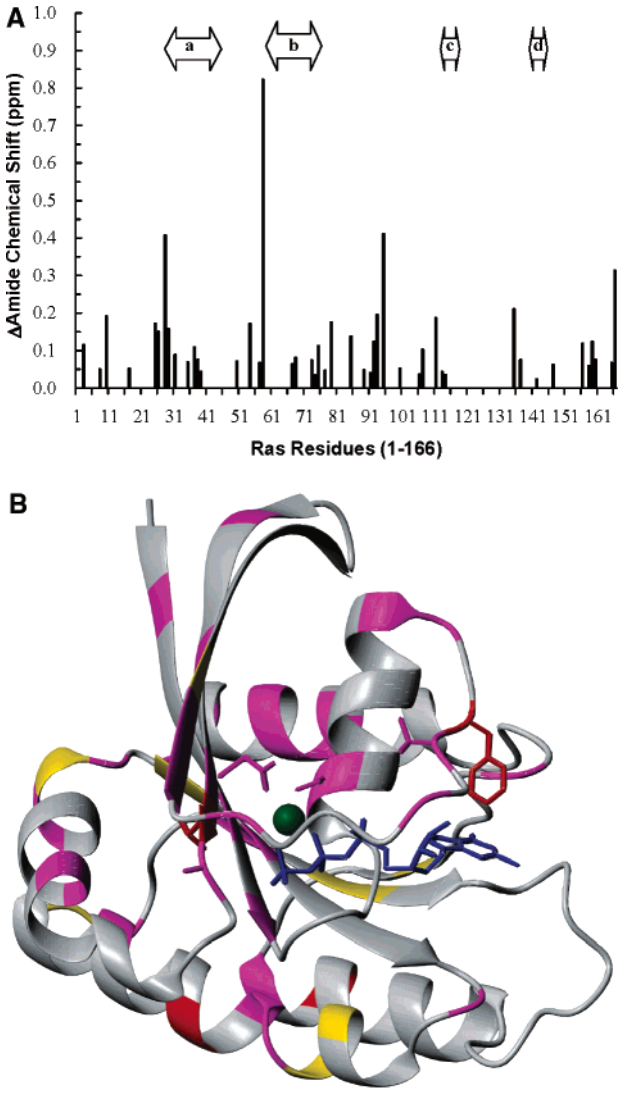

FIGURE 2: pH-dependent wild-type Ras chemical shift changes. (A) NH chemical shifts ($\Delta\delta$) of Ras residues as a function of pH 5.9−8.0 were calculated using eq 1. Arrow bars denoted as a−d represent switch I, switch II, the Ras NKCD motif, and the Ras SAK motif, respectively. (B) Ribbon diagram of Ras highlighting pH-sensitive H_Ns. The NH chemical shifts shown in panel A were categorized into four groups, negligible (∼0.00 ppm), small (∼0.00−0.05 ppm), medium (0.05−0.20 ppm), and large (>0.20 ppm) changes, which are represented in gray, gold, magenta, and red, respectively. Nucleotide and Mg^{2+} are colored blue and green, respectively. This figure was generated using MOLMOL (*28*) using Ras PDB entry 1QRA.

residues (Figure 5). The carbonyl oxygen of Asp^{30} is unusually close to its carboxyl side chain with a distance of 2.49 Å. Moreover, the H_Ns for Asp^{30} and Val^{29} are tightly packed with a hydrogen atom on the side chain of Phe^{28} at a distance of 2.05 and 2.12 Å, respectively, and the phenyl side chain of Phe^{28} packs perpendicular to the guanine base via a stabilizing hydrophobic interaction (Figure 5). Although it is intriguing to speculate that the electrostatic interactions between Asp^{30}/Val^{29} H_Ns and the side chain hydrogen atom of Phe^{28} are perturbed by pH ($^{appNH}pK_a$ estimated to be <5.9), the pH dependence of such interactions has not yet been investigated, and thus, further studies are required to determine whether pH perturbations of these interactions affect Ras·Mg^{2+}·GDP binding interactions.

Thr^{35} is within the Ras switch I region and possesses a small pH-sensitive NH chemical shift and fast H_N exchange rate. Interestingly, while the Thr^{35} NH forms a hydrogen bond interaction with a GTP γ-phosphate oxygen atom in Ras·Mg^{2+}·GTP complexes, this interaction is not present in Ras·Mg^{2+}·GDP complexes. Hence, it is likely that the pH dependence and H_N exchange rate associated with Thr^{35} will differ between GTP- and GDP-bound forms of Ras (*22*). In both the NMR (PDB entry 1AA9) and X-ray structures (PDB entries 1Q21 and 4Q21) of Ras·Mg^{2+}·GDP, Thr^{35} is further removed from the guanine nucleotide-binding pocket but the distance varies in all three structures. This likely reflects increased dynamics of loop 2 in Ras·Mg^{2+}·GDP versus Ras·Mg^{2+}·GTP complexes (*22*). Given the weak pH dependence and $^{appNH}pK_a$ of 6.2, the pH sensitivity of the Thr^{35} NH may reflect transient hydrogen bond interactions, either directly or indirectly with Mg^{2+}-bound H_2O.

Analysis of pH-Dependent NH Chemical Shifts Associated with Ras Residues in the P-Loop and the Switch II Region. Our NMR results indicate that the NH backbone resonances of Ras switch II residues involved in interactions with Mg^{2+} are susceptible to H^+-mediated chemical shift perturbation. Analysis of NMR solution structures (PDB entries 1AA9, 1CRQ, and 1CRR) indicates that side chains of Ser^{17} in the P-loop and Asp^{57} in the switch II DxxG motif form interactions with the nucleotide α- and β-phosphates as well as Mg^{2+}, either directly and indirectly via water molecules. The analysis also shows that the distances from the side chain of Asp^{57} to H_Ns of Asp^{57} and Thr^{58} are 2.68 and 2.07 Å, respectively. We have not been able to observe the carboxyl side chain resonance associated with Asp^{57} in H(CA)CO experiments modified for detection of side chain carboxyl groups (data not shown). Our inability to detect this resonance may be due to chemical exchange of Mg^{2+} from Ras·GDP (*20*, *21*) resulting in line broadening of the Asp^{57} ^{13}C carboxyl resonance. We postulate that the Asp^{57} side chain exists primarily in its carboxylate form over the pH range from 5.9 to 8.0 (Figure 5), since the protonated from (carboxylic acid) of the Asp^{57} side chain is unlikely to form multiple hydrogen bonds with NHs of Asp^{57} and Thr^{58} or a proton of the hydroxyl group of Ser^{17}. If the pK_a of the Asp^{57} side chain is approximately 4, the Asp^{57} side chain will be deprotonated over the pH range that is being investigated, and the $^{appNH}pK_a$ values derived from the pH dependence of both the Asp^{57} and Thr^{58} NH resonances will not be significantly influenced by their hydrogen bond interactions with the Asp^{57} side chain carboxylate. Indeed, $^{appNH}pK_a$ values of Asp^{57} and Thr^{58} are estimated to be 7.2 and 6.8, respectively, which do not correlate with the lower pK_a (presumably ∼4) associated with an Asp side chain (Table 1).

Although we cannot eliminate the possibility that the Asp^{57} side chain titrates in the pH range that is being studied, the most reasonable candidate that can account for the pH sensitivity of the Asp^{57} and Thr^{58} NH resonances is Mg^{2+}-bound H_2O. A possible pK_a range for the titratable Mg^{2+}-bound H_2O is 6.8−7.2, since the $^{appNH}pK_a$ values estimated from NH chemical shifts of Asp^{57} and Thr^{58} are 6.8 and 7.2, respectively (Table 1). Both Ras crystal and NMR solution structures clearly depict a link between Mg^{2+}, the Asp^{57} side chain, and the β-phosphate of Ras-bound GDP. As shown in Figure 5, the H_Ns of Asp^{57} and Thr^{58} have been predicted

Table 1: Determination of Apparent NH pK_a Values for pH-Sensitive H_Ns and Rates of NH Exchange for Residues Involved in Nucleotide Binding

region	residue	total chemical shift (ppm)[a]	$^{appNH}pK_a$[b]	k_{ex}[c] ($\times 10^{-3}$ min^{-1})	region	residue	total chemical shift (ppm)[a]	$^{appNH}pK_a$[b]	k_{ex}[c] ($\times 10^{-3}$ min^{-1})
	M[1]	~0.0000	ND[d]	>150.00		I[84]	~0.0000	ND[d]	~0.00
	T[2]	~0.0000	ND[d]	>150.00		N[85]	0.1386	NM[e]	~0.00
	E[3]	0.1156	NM[e]	>150.00		N[86]	~0.0000	ND[d]	0.03
	Y[4]	~0.0000	ND[d]	>150.00		T[87]	~0.0000	ND[d]	0.26
	K[5]	~0.0000	ND[d]	>150.00		K[88]	~0.0000	ND[d]	~0.00
	L[6]	~0.0000	ND[d]	0.98		S[89]	0.0489	NM[e]	0.14
	V[7]	~0.0000	ND[d]	0.07		F[90]	~0.0000	ND[d]	0.11
	V[8]	0.0503	NM[e]	~0.00		E[91]	0.0415	>8.0	0.33
	V[9]	~0.0000	ND[d]	0.08		D[92]	0.1241	<5.9	0.21
nucleotide phosphate-binding residues	G[10]	0.1922	NM[e]	0.01		I[93]	0.0010	6.9 ± 2.1	2.61
	A[11]	~0.0000	ND[d]	4.56		H[94]	0.0113	6.3 ± 1.6	~0.00
	G[12]	~0.0000	ND[d]	0.61		Q[95]	0.4111	7.2 ± 1.2	~0.00
	G[13]	~0.0000	ND[d]	~0.00		Y[96]	0.0002	ND[d]	12.23
	V[14]	~0.0000	ND[d]	8.12		R[97]	~0.0000	ND[d]	~0.00
	G[15]	~0.0000	NM[e]	0.15		E[98]	~0.0000	ND[d]	~0.00
	K[16]	0.0001	NM[e]	0.34		Q[99]	~0.0000	ND[d]	~0.00
	S[17]	0.0522	7.2 ± 2.7	0.61		I[100]	0.0530	NM[e]	~0.00
	A[18]	~0.0000	ND[d]	0.69		K[101]	~0.0000	ND[d]	0.60
	L[19]	~0.0000	ND[d]	~0.00		R[102]	~0.0000	ND[d]	~0.00
	T[20]	~0.0000	ND[d]	0.11		V[103]	~0.0000	ND[d]	9.06
	I[21]	~0.0000	ND[d]	~0.00		K[104]	~0.0000	ND[d]	~0.00
	Q[22]	~0.0000	ND[d]	0.08		D[105]	~0.0000	ND[d]	~0.00
	L[23]	~0.0000	ND[d]	~0.00		S[106]	0.0366	NM[e]	~0.00
	I[24]	~0.0000	ND[d]	0.34		D[107]	0.1028	NM[e]	~0.00
	Q[25]	0.1726	7.3 ± 1.4	>150.00		D[108]	~0.0000	ND[d]	~0.00
	N[26]	0.1508	6.8 ± 1.3	53.45		V[109]	~0.0000	ND[d]	~0.00
	H[27]	0.0129	<6.2	2.55		P[110]	ND[d]	ND[d]	ND[d]
	F[28]	0.4077	<5.9	>150.00		M[111]	0.1869	NM[e]	~0.00
	V[29]	0.1581	<5.9	>150.00		V[112]	~0.0000	ND[d]	~0.00
	D[30]	0.0486	<5.9	>150.00		L[113]	0.0440	NM[e]	0.22
	E[31]	0.0890	7.1 ± 2.9	>150.00		V[114]	0.0359	NM[e]	0.09
switch I	Y[32]	~0.0000	ND[d]	>150.00		G[115]	~0.0000	ND[d]	0.02
	D[33]	~0.0000	ND[d]	>150.00	NKCD motif	N[116]	~0.0000	ND[d]	0.89
	P[34]	ND[d]	ND[d]	ND[d]		K[117]	~0.0000	ND[d]	0.07
	T[35]	0.0696	6.2 ± 2.2	>150.00		C[118]	~0.0000	ND[d]	0.23
	I[36]	0.0112	7.1 ± 1.9	>150.00		D[119]	~0.0000	ND[d]	0.63
	E[37]	0.0194	<5.9	>150.00		L[120]	~0.0000	ND[d]	0.60
	D[38]	0.0265	<5.9	>150.00		A[121]	~0.0000	ND[d]	1.54
	S[39]	0.0443	<5.9	>150.00		A[122]	~0.0000	ND[d]	1.48
	Y[40]	~0.0000	ND[d]	>150.00		R[123]	~0.0000	ND[d]	30.78
	R[41]	~0.0000	ND[d]	1.68		T[124]	~0.0000	ND[d]	~0.00
	K[42]	~0.0000	ND[d]	~0.00		V[125]	~0.0000	ND[d]	~0.00
	Q[43]	~0.0000	ND[d]	5.21		E[126]	~0.0000	ND[d]	48.10
	V[44]	~0.0000	ND[d]	~0.00		S[127]	~0.0000	ND[d]	~0.00
	V[45]	~0.0000	ND[d]	~0.00		R[128]	~0.0000	ND[d]	~0.00
	I[46]	~0.0000	ND[d]	~0.00		Q[129]	~0.0000	ND[d]	~0.00
	D[47]	~0.0000	ND[d]	0.44		A[130]	~0.0000	ND[d]	~0.00
	G[48]	~0.0000	ND[d]	~0.00		Q[131]	~0.0000	ND[d]	4.46
	E[49]	0.0718	7.4 ± 1.1	~0.00		D[132]	~0.0000	ND[d]	1.43
	T[50]	~0.0000	ND[d]	5.61		L[133]	~0.0000	ND[d]	~0.00
	C[51]	~0.0000	ND[d]	~0.00		A[134]	~0.0000	ND[d]	0.01
	L[52]	~0.0000	ND[d]	0.03		R[135]	0.2118	NM[e]	0.19
	L[53]	~0.0000	ND[d]	1.04		S[136]	~0.0000	ND[d]	9.85
	D[54]	0.1721	6.5 ± 1.6	~0.00		Y[137]	0.0754	NM[e]	2.45
	I[55]	~0.0000	ND[d]	~0.00		G[138]	~0.0000	ND[d]	~0.00
	L[56]	~0.0000	ND[d]	~0.00		I[139]	~0.0000	ND[d]	0.00
	D[57]	0.0676	7.2 ± 2.6	0.94		P[140]	ND[d]	ND[d]	ND[d]
switch II	T[58]	0.8232	6.8 ± 1.5	17.19		Y[141]	~0.0000	ND[d]	0.09
	A[59]	0.0549	6.1 ± 2.7	>150.00		I[142]	0.0240	NM	9.29
	G[60]	~0.0000	ND[d]	>150.00		E[143]	~0.0000	ND[d]	0.14
	Q[61]	~0.0000	ND[d]	>150.00		T[144]	~0.0000	ND[d]	3.30
	E[62]	~0.0000	ND[d]	>150.00	SAK motif	S[145]	~0.0000	ND[d]	~0.00
	E[63]	~0.0000	ND[d]	>150.00		A[146]	0.0007	6.3 ± 3.6	~0.00
	Y[64]	~0.0000	ND[d]	>150.00		K[147]	0.0002	6.4 ± 2.0	~0.00
	S[65]	~0.0000	ND[d]	>150.00		T[148]	0.0000	ND[d]	0.41
	A[66]	~0.0000	ND[d]	>150.00		R[149]	~0.0000	ND[d]	~0.00
	M[67]	0.0646	>8.0	>150.00		Q[150]	~0.0000	ND[d]	~0.00
	R[68]	0.0822	NM[e]	>150.00		G[151]	~0.0000	ND[d]	~0.00
	D[69]	~0.0000	ND[d]	>150.00		V[152]	~0.0000	ND[d]	~0.00
	Q[70]	~0.0000	ND[d]	>150.00		E[153]	~0.0000	ND[d]	2.62
	Y[71]	~0.0000	ND[d]	31.37		D[154]	~0.0000	ND[d]	68.77
	M[72]	~0.0000	ND[d]	~0.00		A[155]	~0.0000	ND[d]	79.38
	R[73]	0.0744	NM[e]	~0.00		F[156]	0.1192	NM[e]	0.09

Table I (Continued)

region	residue	total chemical shift (ppm)[a]	$^{appNH}pK_a$[b]	k_{ex}[c] ($\times 10^{-3}$ min^{-1})	region	residue	total chemical shift (ppm)[a]	$^{appNH}pK_a$[b]	k_{ex}[c] ($\times 10^{-3}$ min^{-1})
	T^{74}	0.0348	NM[e]	0.90		Y^{157}	~0.0000	ND[d]	0.05
	G^{75}	0.1130	NM[e]	~0.00		T^{158}	0.0602	NM[e]	~0.00
	E^{76}	~0.0000	ND[d]	7.16		L^{159}	0.1241	NM[e]	0.17
	G^{77}	0.0474	NM[e]	5.58		V^{160}	0.0754	NM[e]	0.07
	F^{78}	~0.0000	ND[d]	~0.00		R^{161}	~0.0000	ND[d]	0.18
	L^{79}	0.1761	NM[e]	~0.00		E^{162}	~0.0000	ND[d]	2.32
	C^{80}	~0.0000	ND[d]	0.04		I^{163}	~0.0000	ND[d]	~0.00
	V^{81}	~0.0000	ND[d]	0.06		R^{164}	~0.0000	ND[d]	0.04
	F^{82}	~0.0000	ND[d]	0.03		Q^{165}	0.0679	NM[e]	23.08
	A^{83}	~0.0000	ND[d]	0.20		H^{166}	0.3139	NM[e]	>150.00

[a] Total NH chemical shifts ($\Delta\delta$) were calculated using eq 1. Errors (standard deviation, SD) for the values presented were less than 0.0002. [b] Chemical shift-based apparent NH pK_a values ($^{appNH}pK_a$) for GDP interaction residues were determined by fitting quantified pH-dependent NH chemical shift changes to the monoprotic Henderson−Hasselbalch equation (detailed in Figure 3). The method used to determine k_{ex} is described in Materials and Methods. R^2 values and the SD for the determined k_{ex} values are greater than 0.9000 and less than 0.01×10^{-3} min^{-1}, respectively. [c] H_N exchange rate. Precise H_N exchange rates for some Ras resonances are unavailable since the H_Ns associated with these residues underwent deuterium exchange by the time the first HSQC spectrum was acquired (20 min). Peak intensities smaller than 5% (0.05 as a fraction) of the original peak intensity were not quantified. The exponential decay equation can be expressed as $F_{NH} = e^{-k_{ex}t}$, where F_{NH}, k_{ex}, and t equal the fraction of the remaining NH peak intensity, the rate of H_N exchange, and time, respectively. This assumption in combination with the exponential decay equation simplified to $0.05 > e^{-k_{ex}t}$. Solving the equation for k_{ex} (where $F_{NH} = 0.05$ and $t = 20$ min) provides approximate rates of fast NH chemical shifts of $>150 \times 10^{-3}$ min^{-1}. [d] Not determined because these residues are not directly involved in the Ras−guanine nucleotide binding interactions. [e] Not measurable because of indistinguishable chemical shifts.

to form hydrogen bonds with the β-phosphate of Ras-bound GDP via the Asp^{57} carboxylate side chain. Therefore, the electronic state of these functional groups, the GDP β-phosphate and the H_Ns of Asp^{57} and Thr^{58}, may influence the pH-dependent NH chemical shifts of Asp^{57} and Thr^{58}. However, as shown in Figure 6, the ^{31}P resonances of Ras-bound GDP do not shift between pH 6.1 and 8.0, indicating that the β-phosphate of Ras-bound GDP is insensitive to pH changes over this pH range. As the oxygen atom of the Ras-bound GDP β-phosphate coordinates the Asp^{57} side chain (Figure 5), alteration of Mg^{2+} binding coordination by mutation of Asp^{57} to alanine is expected to influence the chemical environment of the β-phosphate of Ras-bound GDP and perturb the ^{31}P chemical shifts of Ras-bound β-phosphate. John et al. (*21*), however, have shown that mutation of Asp^{57} to Ala (D57A) in Ras drastically decreases Mg^{2+} binding affinity, resulting in reduced Ras−guanine nucleotide binding affinity, but surprisingly, no significant β-phosphate ^{31}P NMR chemical shifts in Ras D57A were observed (*20*, *21*). We are currently unable to provide a reasonable explanation for the inconsistencies between kinetic and ^{31}P NMR results observed in this study and previous studies (*20*, *21*).

The H_Ns of Ser^{17}, Asp^{57}, and Thr^{58} form multiple hydrogen bond interactions with the Asp^{57} side chain, suggesting that the H_Ns associated with these residues may be less accessible to solvent exchange. Consistent with these analyses, we have observed that Ras nucleotide phosphate-binding residues, including Ser^{17} and Asp^{57}, exhibit slow H_N exchange rates (Table 1). On the other hand, fast H_N exchange rates were observed for Ras H_N resonances (e.g., Ala^{59}) that are not involved in Ras−guanine nucleotide binding interactions. Intriguingly, a moderate H_N exchange rate was observed for the H_N of Thr^{58}. A possible explanation for these observations is that the H_N of Thr^{58} is more solvent-exposed relative to the Asp^{57} H_N, whereas the Asp^{57} H_N is more protected from the solvent than the H_N of Ala^{59}.

Analysis of pH-Insensitive Ras−Guanine Nucleotide Binding Interactions. NH resonances associated with residues in the NKCD/SAK motifs are not perturbed by pH changes over a pH range from 5.9 to 8.0, indicating that interactions between these motifs and the guanine nucleotide ligand are insensitive to pH changes at the physiological pH regime. Moreover, H_Ns associated with residues in the NKCD/SAK motifs exhibit much slower H_N exchange rates than Ras switch I and II residues (Table 1). Despite the fact that the residues in the NKCD/SAK motifs are located in loop regions of Ras, which are generally more accessible to solvent exchange than NHs contained in secondary structure elements (Figure 2B), the NMR results demonstrate that H_N resonances associated with residues in the NKCD and SAK motifs are resistant to pH perturbations under physiological conditions and less accessible to solvent exchange than residues in the switch regions of Ras. Notably, mutations in these conserved guanine nucleotide-binding motifs dramatically reduce guanine nucleotide binding affinity and greatly enhance GDP dissociation rates (*23*−*25*). We therefore propose that binding interactions between Mg^{2+}·GDP and the residues in the NKCD/SAK loops limit the solvent accessibility of residues in the NKCD/SAK motifs, resulting in highly solvent protected HN resonances. The NH resonances corresponding to residues Gly^{15} and Lys^{16} in the P-loop were also fairly insensitive to changes over a pH range of 5.9−8.0 and exhibited slow H_N exchange rates (Table 1), suggesting that the binding interactions between nucleotide phosphate and P-loop residues are also likely to be unaffected by H^+-mediated perturbations in the physiological pH range.

Kinetics of pH-Dependent Dissociation of Mg^{2+} from the Ras·Mg^{2+}·GDP Complex. Our NMR results are further supported by kinetic studies showing that the binding of Mg^{2+} in nucleotide complexes of Ras is susceptible to the H^+-mediated perturbation. As illustrated in Figures 1 and 2, NH resonances corresponding to residues in Ras involved in Mg^{2+} coordination are quite sensitive to changes in pH, indicating that the apparent dissociation constant of Mg^{2+} in Ras nucleotide complexes is pH-dependent (Figure 4A,B). Guanine nucleotide dissociation rates at pH <5.9 could not be measured because of the instability of Ras in this pH range. Hence, the low-pH asymptotic profile (Figure 4B, inset) associated with the apparent pK_a describing dissociation

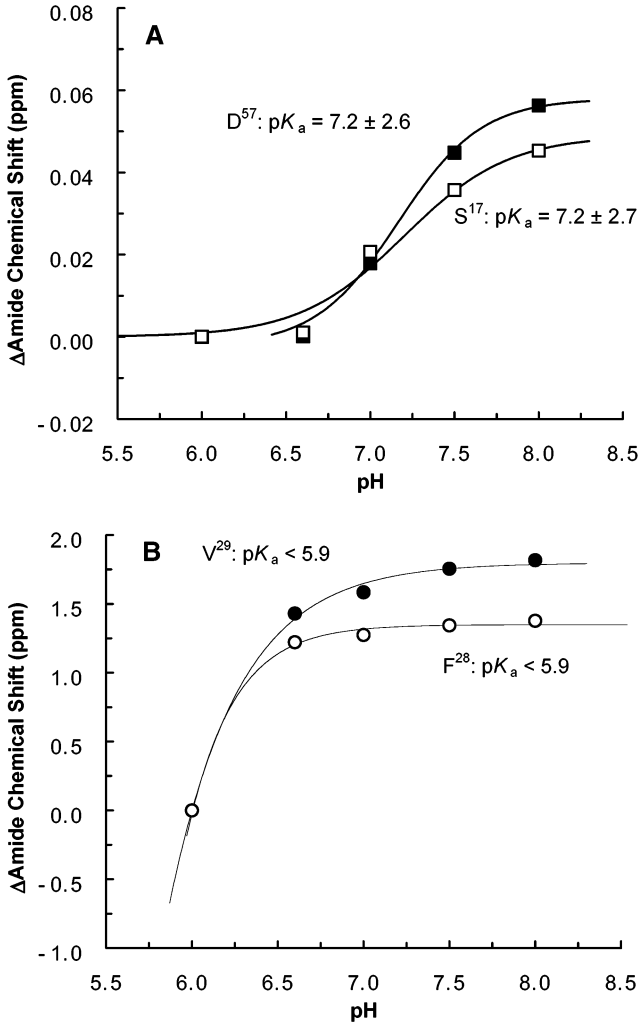

FIGURE 3: Determination of apparent pK_a values for select Ras−guanine nucleotide-binding residues. pH-dependent NH chemical shifts ($\Delta\delta$) for (A) Ser^{17} (□) and Asp^{57} (■) or (B) Phe^{28} (○) and Val^{29} (●) were plotted against pH. The plots were fit to the monoprotic Henderson−Hasselbalch equation to obtain the pH-dependent apparent pK_a ($^{appNH}pK_a$) values for various Ras NHs (*19*). Errors in the $^{appNH}pK_a$ values are denoted with the standard deviation (SD). SD values for $^{appNH}pK_a$ values outside the pH range of 5.9−8.0 were not included, since the estimated values were not fit using the monoprotic Henderson−Hasselbalch equation, but rather estimated from visual estimation.

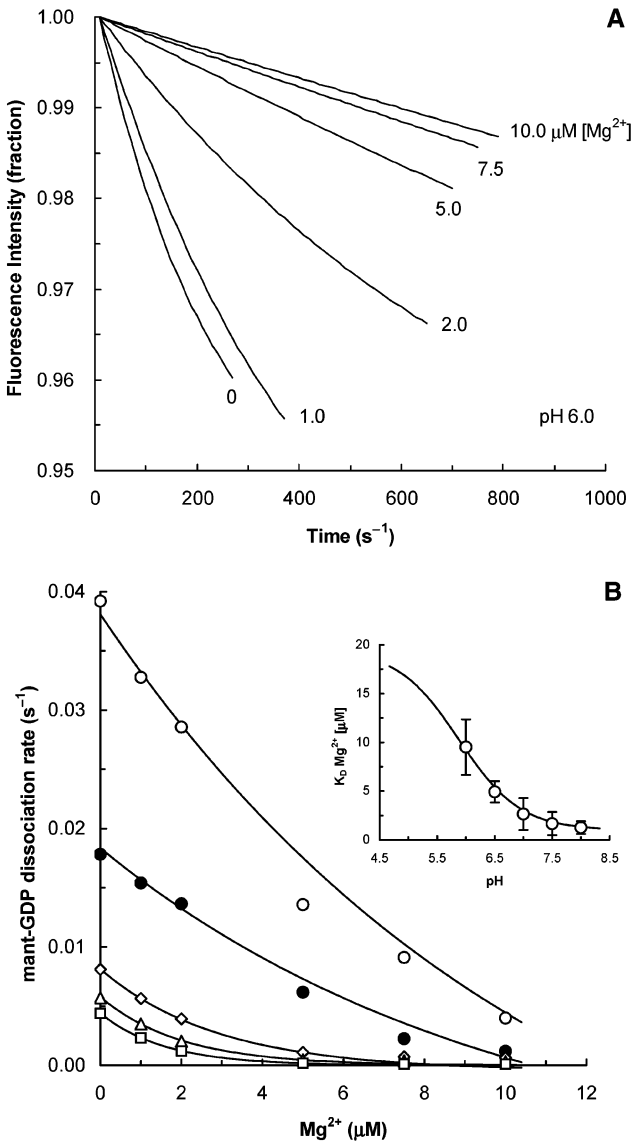

FIGURE 4: Analysis of pH-dependent Ras Mg^{2+} binding affinity. Ras loaded with mant-GDP (1 μM) was transferred into a fluorescence assay cuvette containing unlabeled GDP (20 μM) and various concentrations of Mg^{2+} (0−10 μM) in metal-free mixed buffer. (A) The decrease in fluorescence intensity due to the dissociation of mant-GDP from Ras was monitored over a time period 0−1000 s at 25 °C (pH adjusted at 6.0) (*29*). (B) Mg^{2+} concentration-dependent mant-GDP dissociation of Ras at different pHs was assessed with a procedure identical to that shown in panel A except that the sample pH was varied. The Mg^{2+} concentration-dependent mant-GDP dissociation rates at various pHs were determined by fitting to a single-exponential decay and plotted against concentrations of Mg^{2+}. In the inset, the Mg^{2+} concentration-dependent mant-GDP dissociation rate constants at each pH were fit to an equation for hyperbolic decrease, to estimate the K_D of Mg^{2+} for Ras at various pHs. The K_D of Mg^{2+} for Ras was plotted against pH, and fit to a monoprotic Henderson−Hasselbalch equation (*19*), which gave an apparent pK_a describing dissociation of Mg^{2+} from Ras ($^{app}pK_{D-Mg}$) of 5.9 ± 2.1 ($R^2 = 0.9454$). A best-fit plot using the Henderson−Hasselbalch equation, with an $^{app}pK_{D-Mg}$ of 5.9, is enforced, and only the asymptotes are allowed to float.

of Mg^{2+} from Ras nucleotide complexes ($^{app}pK_{D-Mg}$) does not allow accurate determination of this $^{app}pK_{D-Mg}$ value. Notwithstanding, the $^{app}pK_{D-Mg}$ value estimated in this study is comparable to the previously determined apparent monoprotic pK_a describing dissociation of GDP from Ras nucleotide complexes ($^{app}pK_{D-GDP}$) (*12*). We therefore suggest that pH-mediated perturbation of binding of Mg^{2+} from Ras correlates with pH-dependent nucleotide dissociation from Ras.

DISCUSSION

Ras GTPase activity is believed to be primarily regulated by factors that modulate guanine nucleotide binding affinity (GEFs and NO) or GTPase activity (GAPs) (*6*−*8*). In this study, we have investigated the relationship between pH, NH solvent protection, Mg^{2+} binding affinity, and Mg^{2+}·GDP binding affinity to better understand how Ras GNE is regulated by GEFs and NO. Moreover, our results provide additional insights into Ras−GAP binding interactions that promote enhanced Ras−GTP hydrolysis.

pH-Sensitive Ras Residues and Relevance to Ras GEF-Mediated GNE. The Ras-specific GEF, SOS (Son of sevenless), regulates Ras activity by facilitating Ras GNE (*7*).

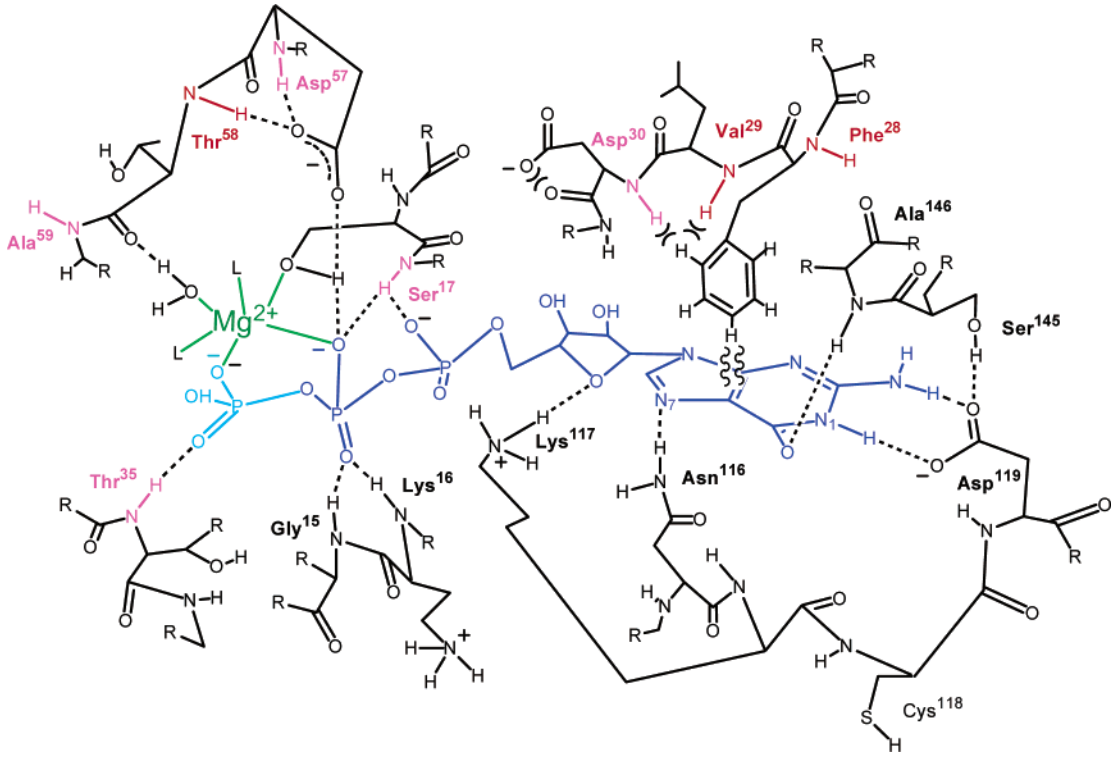

FIGURE 5: Schematic view of Ras−GDP (GTP) interactions. pH-sensitive NHs within Ras are shown in magenta (<0.05−0.20 ppm) and red (>0.20 ppm). Mg^{2+} ion and its coordination with water molecules are shown in green, while GDP is in blue and the γ-phosphate of GTP in sky blue. Hydrogen bond interactions are shown as dashed lines. Aromatic−aromatic interaction between the Phe^{28} side chain and guanine nucleotide base is shown as a pair of wavy lines, and putative electrostatic repulsive interactions between Val^{29} and Asp^{30} are represented by)(. Mg^{2+} coordinates six ligands in the Ras NMR solution structure (PDB entry 1AA9); some of the Mg^{2+}-coordinated ligands were expressed as L. The nucleotide interaction with Ras residue Lys^{147} was omitted for convenience. The schematic presentation of Ras residues involved in interactions with Mg^{2+}·guanine nucleotide ligands (Mg^{2+}·GDP and Mg^{2+}·GTP) is based on the NMR solution structure 1AA9 (GDP·Mg^{2+}·Ras complex) and X-ray crystal structure 1QRA (GTP·Mg^{2+}·Ras complex), although atomic distances and their relative positions were changed arbitrarily for presentation.

Although structures of SOS−Ras complexes corresponding to the various reaction steps are not available, a mechanism for SOS-mediated GNE on Ras has been proposed on the basis of the crystal structure of Ras in a binary complex with the SOS Ras GEF domain combined with kinetic data on wild-type and mutant proteins (*7*, *26*). In the proposed mechanism, the binding of the SOS GEF domain to Ras causes structural perturbations in switch I due to insertion of two helices (H and I) from SOS. In addition, insertion of side chains of Leu^{938} and Glu^{942} from the SOS GEF domain into the Ras switch II region destabilizes the Ras-bound nucleotide by perturbing Mg^{2+} coordination as well as the spatial orientation of Lys^{16} in the P-loop, a residue connected to Ser^{17}. The data, taken together, suggest that association of the SOS GEF domain with Ras competes with Mg^{2+}·guanine nucleotide interactions, thereby promoting release of the bound Mg^{2+}·guanine nucleotide ligand from Ras.

Our NMR results indicate that residues in switch I (Phe^{28}−Asp^{30}) as well as residues involved in Mg^{2+} binding (Asp^{57} and Thr^{58} in switch II and P-loop residue Ser^{17}) are solvent accessible and sensitive to physiological pH changes. Intriguingly, perturbations are observed in these same residues upon SOS binding to Ras, indicating that certain residues in the switch I and II regions of Ras may impart an energetically favorable binding milieu necessary for SOS-mediated GNE of Ras.

Our results indicate that pH-sensitive NH resonances associated with the Ras switch I region possess an $^{appNH}pK_a$ of <5.9, whereas the NH resonances corresponding to Ras residues that coordinate Mg^{2+}-bound water in the switch II region possess neutral $^{appNH}pK_a$ values. We anticipated that the apparent pK_a describing dissociation of Mg^{2+} from Ras nucleotide complexes, the $^{app}pK_{D-Mg}$, would correlate with the $^{appNH}pK_a$ values for residues in the switch II region, since the primary Mg^{2+} coordination residues critical for high-affinity Ras−guanine nucleotide binding interactions are located in the Ras switch II region (*20*, *21*). However, the $^{app}pK_{D-Mg}$ value of 5.9 shows a better correlation with the $^{appNH}pK_a$ for pH-sensitive NH resonances corresponding to residues in switch I. A possible explanation for these results is that H^+-mediated perturbation of the switch I region may alter the conformation of switch II. This may, in turn, perturb Ras·Mg^{2+}·nucleotide ligand binding interactions resulting in release of Mg^{2+}, thus enhancing dissociation of guanine nucleotide from Ras. Further studies will be required to elucidate how the conformation of the Mg^{2+}-coordinated residues in switch II may be affected by pH-sensitive residues in the switch I region of Ras.

pH-Sensitive NH Resonances in Ras and Relevance to NO-Mediated Ras GNE. We have recently investigated the mechanism by which NO mediates Ras GNE, and found that it proceeds by a radical-based mechanism (*12*). We have proposed that reaction of NO in the presence of O_2 produces $^{\bullet}NO_2$, which then reacts with the Ras Cys^{118} thiol (Ras-$S^{118}H$) to produce a Ras−thiyl radical intermediate (Ras-$S^{118\bullet}$) and a H^+. The Ras-$S^{118\bullet}$, in turn, reacts with NO to produce S-nitrosylated Ras (Ras-$S^{118}NO$). We have further shown that it is the Ras radical intermediate, proposed to be Ras-$S^{118\bullet}$,

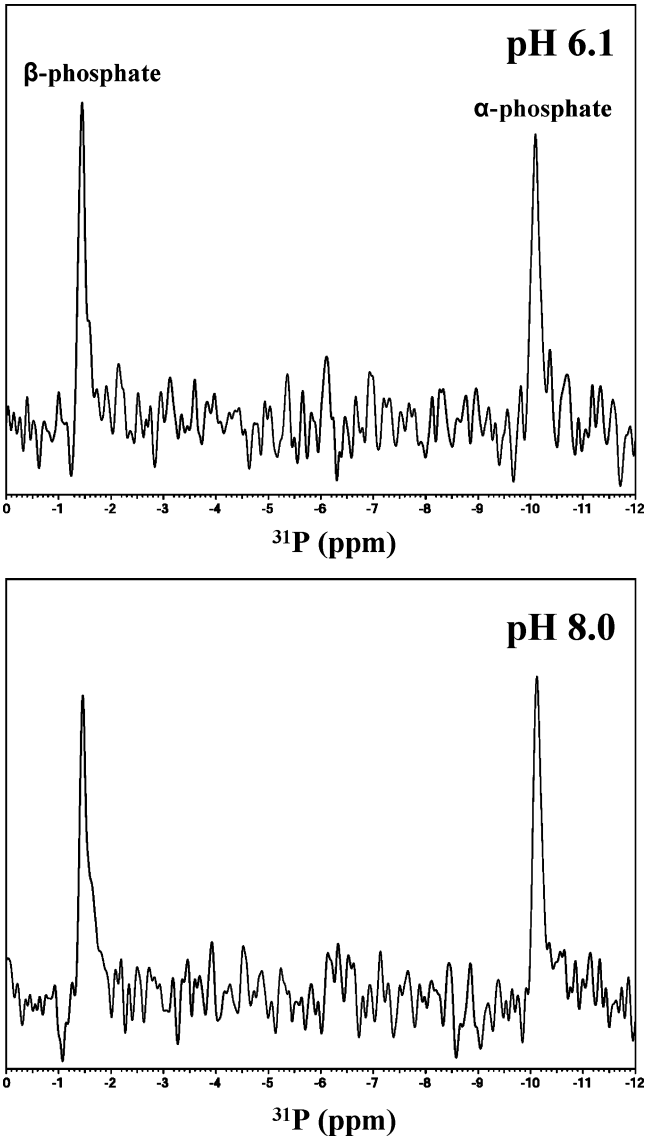

FIGURE 6: ^{31}P spectra of Ras-bound GDP. Resonances corresponding to the α- and *β*-phosphates of GDP at pH 6.1 and 8.0 are indicated.

not the Ras-S^{118}NO end product, that promotes NO-mediated Ras GNE under aerobic conditions. The Ras-S^{118}H pK_a is expected to be similar to those of free cysteine and glutathione (p$K_a \sim 9$) (*19*), since the Ras-S^{118}H thiol moiety is highly solvent exposed in wild-type Ras structures (*9*, *10*). Therefore, at the physiological pH (i.e., pH 7.5), the Ras Cys^{118} thiol group most likely exists as a thiol (Ras-S^{118}H) rather than a thiolate (Ras-S^{118-}). Given the solvent accessibility of the Ras-S^{118}H thiol side chain and the redox potential of free thiols (*27*), it is likely that $^{\bullet}NO_2$ directly reacts with Ras-S^{118}H to produce Ras-S$^{118\bullet}$ and a H^+ byproduct. However, since free thiolates have lower redox potentials than free thiols (*27*), it is possible that, under our experimental conditions, the thiol moiety of Ras-S^{118}H dissociates to Ras-S^{118-} and H^+ prior to reaction with $^{\bullet}NO_2$, to produce Ras-S^{118}NO. Notwithstanding, although we favor the radical-based mechanism for Ras NO modification as detailed above, it is important to note that all possible S-nitrosylation mechanisms that have been proposed produce a H^+ (derived from the reactive SH) as a reaction byproduct (*12*). If pH-independent mechanisms of nitrosothiol formation exist, such reactions are unlikely to perturb pH-dependent Ras−guanine nucleotide binding interactions.

Since the H^+-producing site on Ras, Ras-S^{118}H, is contained within the NKCD/SAK motifs of Ras and forms critical hydrogen bond interactions with the guanine base, we previously proposed that the H^+ byproduct may participate in promoting Ras GNE by perturbing these interactions (*12*). To delineate the role of the H^+ byproduct in NO-mediated Ras GNE, we conducted a comparative kinetic analysis of Ras−guanine nucleotide dissociation rates as a function of pH in the presence and absence of $^{\bullet}NO_2$ (*12*). Results from this study showed that whereas stimulation of Ras−guanine nucleotide dissociation by $^{\bullet}NO_2$ treatment (∼1 *μ*M) was significant (>100-fold), the observed enhancement in guanine nucleotide dissociation as a function of pH (2 pH units, from 8.0 to 5.9) was reduced ∼10-fold relative to that observed in the presence of $^{\bullet}NO_2$ (GNE stimulated ∼15-fold). These results indicate the $^{\bullet}NO_2$-mediated Ras−guanine nucleotide dissociation is primarily driven by Ras-S$^{118\bullet}$ as opposed to H^+-mediated guanine nucleotide dissociation, yet it was unclear how a reduction in pH from 8 to 5.9 led to stimulation of Ras−guanine nucleotide dissociation. Results obtained from this study demonstrate that hydrogen bond and/or electrostatic interactions between the guanine nucleotide base of GDP and residues in the Ras NKCD/SAK motifs are not sensitive to H^+-mediated perturbation over a pH range from 5.9 to 8.0. In contrast, since the Ras switch I and II regions appear to be sensitive to pH changes, a reduction in pH may perturb pH-sensitive interactions with Mg^{2+}·GDP. These results suggest that H^+s formed by reaction of Ras and $^{\bullet}NO_2$ are unlikely to directly perturb the hydrogen bond interactions between the Ras NKCD/SAK motifs and the guanine nucleotide base. Although it is conceivable that H^+ produced from the reaction of Ras and $^{\bullet}NO_2$ may migrate to the pH-sensitive Ras regions (switch I and II) to perturb Mg^{2+}·guanine nucleotide ligand interactions, it is more likely that H^+s generated from reaction of Ras and NO diffuse away from Ras since the Cys^{118} side chain is exposed to the solvent. Hence, results from these analyses indicate that H^+-mediated enhancement of Ras−guanine nucleotide dissociation (*12*) is most likely due to the titration of pH-sensitive Ras switch I and II functional groups, rather than titration of functional groups contained within the Ras NKCD/SAK motifs.

pH-Sensitive Ras Residues and Relevance to Ras−GAP-Mediated Ras GTPase Activity. The Ras specific GAP, p120^{GAP}, also binds to the switch I and II regions of Ras (*6*). However, the residues in Ras that interact with GAP differ from residues of Ras that interact with SOS. GAP interacts with Ras residues Tyr^{32}, Pro^{34}, and Ile^{36} in the switch I region that overlap with the Ras effector-binding region, as well as Gln^{61}−Tyr^{64} in the switch II region (*6*). In contrast to SOS-interacting Ras residues, however, these GAP-interacting Ras residues show neither pH-sensitive NMR chemical shifts nor fast H_N exchange rates. Unlike SOS, GAP interacts with Ras to enhance Ras GTPase activity, which does not necessarily require perturbation of the binding interactions between the nucleotide ligand and the Ras switch I and II residues. Therefore, previous findings that Ras GAPs do not decrease the affinity between Ras and GDP are consistent with our NMR observations that the NH resonances associated with GAP-interacting residues in Ras are

not solvent accessible and are also insensitive to small changes in pH.

CONCLUSION

On the basis of our results in conjunction with the previous studies, we postulate that electrostatic interactions involving Ras Mg^{2+}-binding residues, in particular, $Phe^{28}-Asp^{30}$ in switch I and Asp^{57} and Thr^{58} in switch II of Ras, appear to be coupled to pH-dependent Ras Mg^{2+} binding and guanine nucleotide binding affinity and thus are sensitive to protein−protein or pH perturbations. Perturbation of Ras−guanine nucleotide binding interactions by these agents leads to enhancement of Ras GNE and modulation of cellular Ras activity.

Results obtained from this study do not provide information regarding hydrophobic interactions between Ras and its Mg^{2+}·guanine nucleotide ligands. Additional investigation of these types of interactions may aid in further elucidating energetic contributions responsible for high-specificity and high-affinity binding interactions between Ras and its Mg^{2+}·guanine nucleotide ligands. This information, in turn, may provide further insights into how various agents modulate Ras nucleotide binding affinity and thus cellular Ras activity.

ACKNOWLEDGMENT

We thank Dr. Yibing Wu for help in acquiring ^{31}P NMR data.

REFERENCES

1. Campbell, S. L., Khosravi-Far, R., Rossman, K. L., Clark, G. J., and Der, C. J. (1998) Increasing complexity of Ras signaling, *Oncogene 17*, 1395−1413.
2. Downward, J., Graves, J., and Cantrell, D. (1992) The regulation and function of $p21^{ras}$ in T cells, *Immunol. Today 13*, 89−92.
3. Shields, J. M., Pruitt, K., McFall, A., Shaub, A., and Der, C. J. (2000) Understanding Ras: 'it ain't over 'til it's over', *Trends Cell Biol. 10*, 147−154.
4. Geyer, M., and Wittinghofer, A. (1997) GEFs, GAPs, GDIs and effectors: taking a closer (3D) look at the regulation of Ras-related GTP-binding proteins, *Curr. Opin. Struct. Biol. 7*, 786−792.
5. Irani, K., and Goldschmidt-Clermont, P. (1998) Ras, Superoxide and Signal Transduction, *Biochem. Pharmacol. 55*, 1339−1346.
6. Scheffzek, K., Ahmadian, M. R., Kabsch, W., Wiesmuller, L., Lautwein, A., Schmitz, F., and Wittinghofer, A. (1997) The Ras-RasGAP complex: structural basis for GTPase activation and its loss in oncogenic Ras mutants, *Science 277*, 333−338.
7. Boriack-Sjodin, P. A., Margarit, S. M., Bar-Sagi, D., and Kuriyan, J. (1998) The structural basis of the activation of Ras by Sos, *Nature 394*, 337−343.
8. Lander, H. M., Milbank, A. J., Tauras, J. M., Hajjar, D. P., Hempstead, B. L., Schwartz, G. D., Kraemer, R. T., Mirza, U. A., Chait, B. T., Campbell-Burk, S. L., and Quilliam, L. A. (1996) Redox regulation of cell signalling, *Nature 381*, 380−381.
9. Milburn, M. V., Tong, L., deVos, A. M., Brunger, A., Yamaizumi, Z., Nishimura, S., and Kim, S. H. (1990) Molecular switch for signal transduction: structural differences between active and inactive forms of protooncogenic ras proteins, *Science 247*, 939−945.
10. Pai, E. F., Krengel, U., Petsko, G. A., Goody, R. S., Kabsch, W., and Wittinghofer, A. (1990) Refined crystal structure of the triphosphate conformation of H-ras p21 at 1.35 Å resolution: implications for the mechanism of GTP hydrolysis, *EMBO J. 9*, 2351−2359.
11. Lander, H. M., Ogiste, J. S., Pearce, S. F., Levi, R., and Novogrodsky, A. (1995) Nitric Oxide-stimulated Guanine Nucleotide Exchange on $p21^{ras}$, *J. Biol. Chem. 270*, 7017−7020.
12. Heo, J., and Campbell, S. L. (2004) Mechanism of p^{21}Ras S-nitrosylation and Kinetics of Nitric Oxide-mediated Guanine Nucleotide Exchange, *Biochemistry 43*, 2314−2322.
13. Heo, J., Staples, C. R., Halbleib, C. M., and Ludden, P. W. (2000) Evidence for a ligand CO that is required for catalytic activity of CO dehydrogenase from *Rhodospirillum rubrum*, *Biochemistry 39*, 7956−7963.
14. Campbell-Burk, S. L., and Carpenter, J. W. (1995) Refolding and purification of Ras proteins, *Methods Enzymol. 255*, 3−13.
15. Johnson, B. A., and Blevins, R. A. (1994) NMR view: a computer program for the visualization and analysis of NMR data, *J. Biolmol. NMR 4*, 603−614.
16. Delaglio, F., Grzesiek, S., Vuister, G. W., Zhu, G., Pfeifer, J., and Bax, A. (1995) NMRPipe: a multidimensional spectral processing system based on UNIX pipes, *J. Biomol. NMR 6*, 277−293.
17. Kraulis, P. J., Domaille, P. J., Campbell-Burk, S. L., Van Aken, T., and Laue, E. D. (1994) Solution structure and dynamics of ras p21·GDP determined by heteronuclear three- and four-dimensional NMR spectroscopy, *Biochemistry 33*, 3515−3531.
18. Arumugam, S., Hemme, C. L., Yoshida, N., Suzuki, K., Nagase, H., Berjanskii, M., Wu, B., and Van Doren, S. R. (1998) TIMP-1 contact sites and perturbations of stromelysin 1 mapped by NMR and a paramagnetic surface probe, *Biochemistry 37*, 9650−9657.
19. Segel, I. H. (1976) *Biochemical calculations*, 2nd ed., John Wiley & Sons, New York.
20. Reinstein, J., Schlichting, I., Frech, M., Goody, R. S., and Wittinghofer, A. (1991) p21 with a phenylalanine 28 → leucine mutation reacts normally with the GTPase activating protein GAP but nevertheless has transforming properties, *J. Biol. Chem. 266*, 17700−17706.
21. John, J., Rensland, H., Schlichting, I., Vetter, I., Borasio, G. D., Goody, R. S., and Wittinghofer, A. (1993) Kinetic and structural analysis of the Mg^{2+}-binding site of the guanine nucleotide-binding protein $p21^{H-ras}$, *J. Biol. Chem. 268*, 923−929.
22. Spoerner, M., Herrmann, C., Vetter, I. R., Kalbitzer, H. R., and Wittinghofer, A. (2001) Dynamic properties of the Ras switch I region and its importance for binding to effectors, *Proc. Natl. Acad. Sci. U.S.A. 98*, 4944−4949.
23. Hwang, Y., Zhong, J., Poullet, P., and Parmeggiani, A. (1993) Inhibition of SDC25 C-domain-induced guanine-nucleotide exchange by guanine ring binding domain mutants of v-H-ras, *J. Biol. Chem. 268*, 24692−24698.
24. Zhong, J. M., Chen-Hwang, M. C., and Hwang, Y. W. (1995) Switching nucleotide specificity of Ha-Ras p21 by a single amino acid substitution at aspartate 119, *J. Biol. Chem. 270*, 10002−10007.
25. Cool, R. H., Schmidt, G., Lenzen, C. U., Prinz, H., Vogt, D., and Wittinghofer, A. (1999) The Ras mutant D119N is both dominant negative and activated, *Mol. Cell. Biol. 19*, 6297−6305.
26. Hall, B. E., Yang, S. S., Boriack-Sjodin, P. A., Kuriyan, J., and Bar-Sagi, D. (2001) Structure-based mutagenesis reveals distinct functions for Ras switch 1 and switch 2 in Sos-catalyzed guanine nucleotide exchange, *J. Biol. Chem. 276*, 27629−27637.
27. Stubbe, J., and van der Donk, W. A. (1998) Protein Radicals in Enzyme Catalysis, *Chem. Rev. 98*, 705−762.
28. Koradi, R., Billeter, M., and Wüthrich, K. (1996) A program for display and analysis of macromolecular structures, *J. Mol. Graphics 14*, 51−55.
29. Lenzen, C., Cool, R. H., Prinz, H., Kuhlmann, J., and Wittinghofer, A. (1998) Kinetic Analysis by Fluorescence of the Interaction between Ras and the Catalytic Domain of the Guanine Nucleotide Exchange Factor $Cdc25^{Mm}$, *Biochemistry 37*, 7420−7430.

BI035704A